Aeroacoustics-based Structural Health Monitoring of Airfoils with Surface Damage and Acoustic Domain-Coupling

Caleb Traylor*, Murat Inalpolat†, and David J. Willis‡

University of Massachusetts Lowell, Lowell, MA, 01854, USA

and

Per-Olof Persson§

University of California, Berkeley, Berkeley, CA, 94720, USA

Lawrence Berkeley National Laboratory, Berkeley, Berkeley, CA, 94720, USA

Nomenclature

L_c = airfoil chord length

s = damage side length

DL = damage location

S = suction side

P = pressure side

SPL = sound pressure level

ΔSPL = change in sound pressure level

I.Introduction

WIND turbine blade monitoring for damage offers significant benefits both in terms of economic savings and sustainability[1-5]. It is critical to identify and repair damage as soon as possible to limit turbine downtime, minimize repair costs, and prevent catastrophic component failure. An acoustics-based approach proposed by Niezrecki and Inalpolat [6] would allow for in-operation turbine blade monitoring via measurement of the blade-internal cavity sound. If the change in blade's structural health status (from healthy to damaged) causes a consistent significant difference in the sound distribution, the wind farm operator can be notified, and the blade can be inspected and repaired. There are two factors that can cause the blade acoustics to change when damage is present. First, the acoustic

* Research Assistant, Department of Mechanical Engineering; AIAA Member.

† Associate Professor, Department of Mechanical Engineering; Murat_Inalpolat@uml.edu (Corresponding Author).

‡ Associate Professor, Department of Mechanical Engineering; AIAA Senior Member.

§ Professor, Department of Mathematics, University of California, Berkeley
Faculty Scientist, Mathematics Group, Lawrence Berkeley National Laboratory; AIAA Senior Member.

transmission loss (TL) will change when an opening is created on the blade skin, as more sound can pass into the blade internal domain. Second, there may be a change in the aeroacoustic sound generated by airflow over the blade when damage is present compared to the sound generated by flow over the healthy blade. The surface discontinuity caused by the damage will affect the flow and thus the spatial and temporal acoustic pressure distribution. Additionally, the opening created by the damage location allows for coupling between the internal and external domains that may create a unique sound.

This acoustics-based SHM approach has been studied both experimentally [1, 7-11] and computationally [12-14]. However, to date, the focus has primarily been on the first factor – the change in transmission loss, not on the sound generated by a damaged blade. Thus far, the only experimental studies that include the sound generated by airflow over the damage location involve wind tunnel experiments using a small blade cross-section [1, 11]. In these studies, Beale at al. demonstrated that damage as small as 0.32 cm in diameter could be detected using an internal cavity microphone[1]. However, these investigations did not isolate the influence of the two individual acoustic factors (change in TL and change in aeroacoustics due to damage). On the computational side, a reduced-order model has been used for aeroacoustic sound generated by flow over a healthy blade, and damage detection prediction has been based on a change in TL to detect damage [12-15]. These investigations were beneficial in demonstrating the SHM approach, but they did not consider damage-induced sound and how it might affect damage detection.

The present investigation serves to fill a critical gap in the previous research into the structural health monitoring approach. While the previous computational investigations modeled the flow-generated sound for flow over a healthy wind turbine blade [12-15], this research will consider the effect of the damage itself on sound generation. A high-order accurate modeling approach to flow-induced sound is used to identify the impact of the damage location itself on the sound that is generated and the effect of the coupling between the external flow domain and the internal blade cavity domain.

II. Methodology

The numerical simulations are based on high-order accurate Discontinuous Galerkin methods, using the in-house software 3DG[16]. While not routinely used for CFD simulations, these high-order methods have been shown to be superior over traditional methods for in particular Large Eddy Simulation due to their low numerical dissipation [17, 18]. In addition, for strongly coupled aeroacoustic phenomena like the ones in this work, it is widely believed that due to their high numerical dissipation low-order methods are unable to efficiently capture small pressure perturbations using direct numerical simulation of the Navier-Stokes equations.

The fully compressible Navier-Stokes equations are solved directly, without any models for the turbulence or the acoustics. Since the mesh is not resolving all the scales, this corresponds to an Implicit Large Eddy Simulation (ILES) technique where the inherent dissipation of the numerical scheme is used as a subgrid model. While the pros and cons of such an approach can be discussed, it is routinely used and has been highly successful for prediction of massively separated flow using high-order methods[19].

In all simulations, tetrahedral elements with polynomial degree p = 3 are used for the spatial discretization. In time, an L-stable 3-stage, 3rd order accurate DIRK scheme is used. The large non-linear systems that arise are solved with a preconditioned Newton-GMRES method, implemented in parallel using standard domain decomposition [16].

The NACA 0012 airfoil is used in this study as a representative case. All dimensions were normalized such that the airfoil chord length $L_c = 1$. The trailing edge had a thickness of $0.00252L_c$. As shown in Fig. 1(a), an internal domain was defined from x = $0.3L_c$ to x = $0.8L_c$ using a smaller NACA 0012 airfoil. Only a single internal acoustic cavity was included in the model. Since this computational approach does not include structural coupling, it was not necessary to include any other cavities that may be separated by shear webs. Based on previous research, there is expected to be limited acoustic coupling between the blade internal cavities [13]. Thus, although in practice there may be a small opening connecting the cavities at the root and tip of the blade, this was not likely to be worth the additional computational cost of the increased domain size. Also shown in Fig. 1(a) are the four representative damage locations used in this investigation. These locations were investigated one at a time such that each damage model only consisted of one of the four damage cases. Each damage case was square-shaped with a side length of $s_{damage} = 0.025L_c$. Damage location DL1 begins at an x-location of $0.35L_c$, while damage location DL2 begins at $x = 0.55L_c$. Two of the damage cases were located on the suction (S) side of the airfoil, and the other two were located on the pressure (P) side.

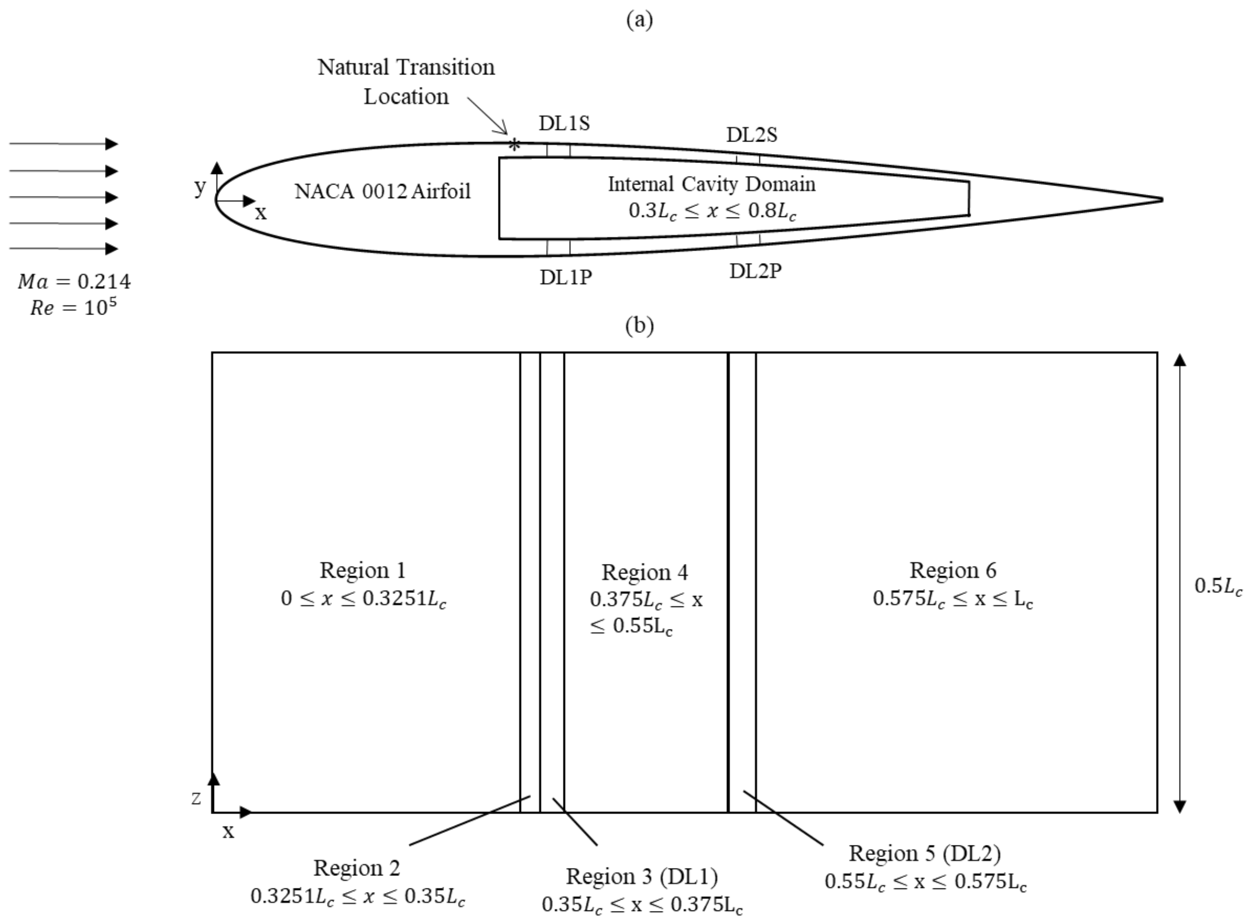

Fig. 1 (a) Airfoil geometry in x-y plane showing damage locations (DL), internal domain, and natural transition location on suction side (b) Overhead view (x-z plane) showing six regions for grouping of external domain pressure probes.

Adiabatic no-slip conditions were imposed on the airfoil surface with characteristic boundary conditions at all the far-field boundaries. Periodic boundary conditions were applied on the x-y faces of the external domain such that the external flow extended infinitely in the z-direction despite only modeling an external span of $0.5L_c$. For the internal domain, the span was finite, and no-slip boundary conditions were applied at the walls. Two internal domain (ID) cases were considered in order to investigate the change in acoustic content created by the coupling of the internal and external domains separate from the change created by the surface discontinuity. First, the *Small ID* case has an internal domain with a span of $0.5L_c$. This smaller geometry was useful for efficient comparison of different damage locations. Second, there is a *Large ID* internal domain case, which is closest to the actual wind turbine blade geometry. This case has a total internal domain span of $10L_c$ as the internal domain is expanded by $4.75L_c$ in both the positive and negative z-directions.

The flow speed and angle of attack were selected based on the flow conditions toward the tip of a wind turbine blade used in previous computational investigations[13, 14]. For the inlet flow, a Mach number (*Ma*) of 0.214 was selected, which corresponds to a flow speed of 73.5 m/s, at an angle of attack of 5°. However, due to high mesh requirements, the Reynolds number was limited to 10^5 to keep computational costs down and to ensure the flow was in a regime that had been previously shown to be accurately modeled by LES on medium fine grids such as the ones used in this work. Thus, this would indicate a higher viscosity of the fluid than that of air. In future work, it may be worthwhile to investigate the effect of increasing the Reynolds number, as the flow will transition to turbulent closer to the leading edge for higher *Re* values.

The acoustic pressure was measured at select virtual pressure probe locations throughout the flow domain. Since there were more probes than could be examined individually, the external domain probes were divided into groups by region along the chord length of the airfoil as shown in Fig. 1(b). There were six regions along the airfoil from leading edge to trailing edge, in addition to two separate groups for the probes located upstream of the leading edge or downstream of the trailing edge. Since the mesh increased in size away from the airfoil, only the probes for which $|y| < 0.1L_c$ were considered in this analysis. For the regions along the airfoil chord length, the dividing lines were the XFOIL [20] prediction for natural transition ($x = 0.3251L_c$), the DL1 boundaries ($x = 0.35L_c$ and $x = 0.375L_c$), and the DL2 boundaries ($x = 0.55L_c$ and $x = 0.575L_c$) as shown in Fig. 1(b). These regions were also separated between pressure side probes and suction side probes. To quantify the change in acoustic pressure when damage was present, the change in sound pressure level, ΔSPL, was calculated according to Eq. 1.

$$\Delta SPL = SPL_{Damaged} - SPL_{Healthy} \tag{1}$$

III. Results and Discussion

With the higher-order approach, this investigation represented the first time that the damage-generated sound was modeled computationally. For the baseline healthy case, no sound was modeled in the internal domain, as the acoustic and flow domains were completely separated. Once damage was introduced (see Fig. 2), air flowing over the damage side of the airfoil entered the internal cavity, creating a coupling effect. In the rest of this results section, we will discuss the effect of this coupling both on the external sound near the airfoil boundary and on the blade-internal cavity sound.

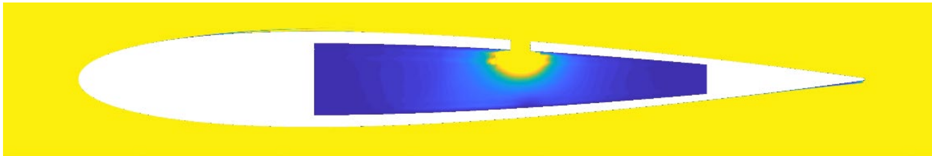

Fig. 2 Velocity contour plot showing airflow entering blade internal cavity for damage case DL2S (yellow = free-stream velocity; blue = zero velocity).

First, the impact of the damage location was investigated by modeling the four damage locations depicted previously in Fig. 1. The small internal domain was used for these simulations in order to conserve computational resources. The effect of internal domain size will be studied in the next section. The *ΔSPL* values are shown in Fig. 3 for the suction side and Fig. 4 for the pressure side. Looking at Fig. 3 for the suction side first, it is clear that the damage location DL1S has the greatest impact on the external domain sound. This is likely due to the fact that this damage is placed near the natural (theoretically expected) location for transition to turbulent flow. The increase in *SPL* is most noticeable in the external domain for regions prior to the full transition to turbulent flow. In Region 1, where the flow is laminar, damage location DL2S also caused a significant increase in *SPL*, with a median change of 5.4 dB. Even damage case DL1P caused a notable median increase of 3.1 dB in this region. However, once the flow is fully turbulent in Regions 4-6, there is no longer a notable increase in *SPL* or much change between damage locations. The change is most easily identified in the laminar region on the suction side of the airfoil, even if the damage itself is in the turbulent region, as in the case of DL2S.

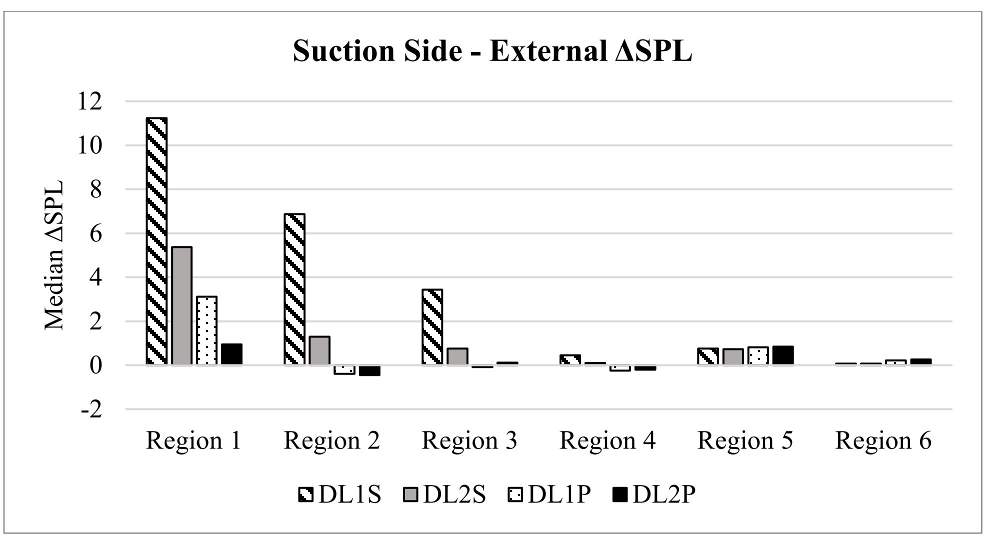

Fig. 3 Median ΔSPL values for the Small Internal Domain case for the airfoil suction side for all four damage locations

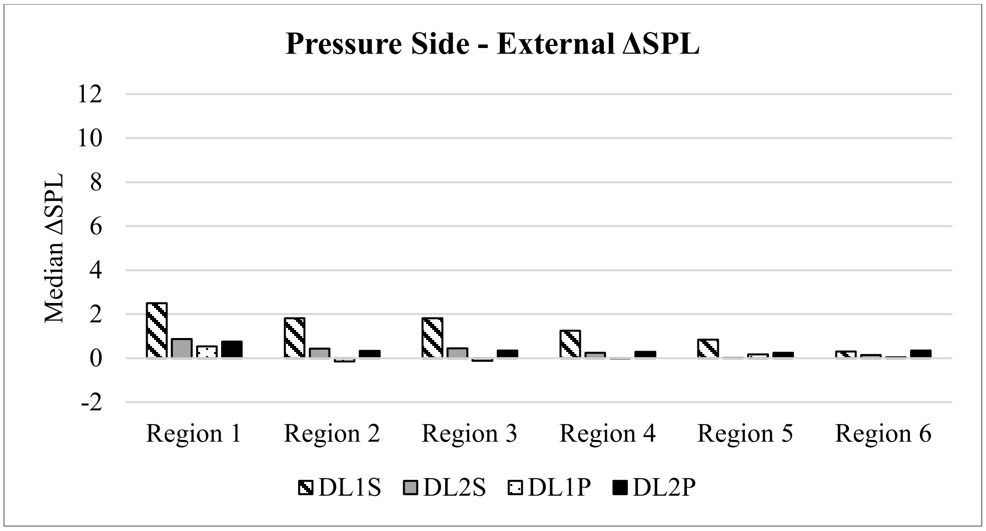

Fig. 4 Median ΔSPL values for the Small Internal Domain case for the airfoil pressure side for all four damage locations

The pressure side results revealed by Fig. 4 highlights that even for the pressure-side damage locations DL1P and DL2P, there was not a significant increase in *SPL*. These results indicate that damage in the laminar flow region would be more difficult to detect if detection were solely dependent on aeroacoustic noise. Damage in this region may still be detectable due to a change in transmission loss and measurement of sound from other acoustic sources beyond the aeroacoustic noise, which is outside the scope of this paper.

The effect of the size of the internal domain was investigated for the two suction-side damage cases. Since the healthy case did not have any sound transmitted to the internal domain, it is not possible to calculate *ΔSPL* for the internal domain. Instead, the median *SPL* for the internal domain pressure probes is shown in Fig. 5. The same pressure probe locations were used for both internal domain sizes for the sake of comparison, and the internal cavity sound was much louder (higher acoustic pressure levels were observed) for the smaller domain size. This is likely due to the reverberations that die out in the larger cavity, and indicates that damage will likely be easier to detect for internal cavity microphones placed in smaller cavities compared to those in larger cavities. This fact will continue to be monitored in future work.

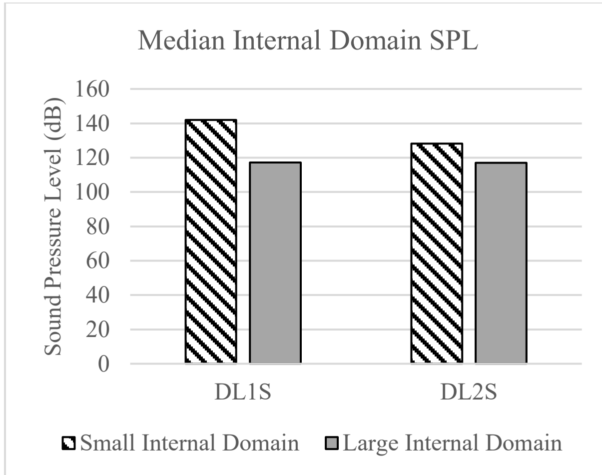

Fig. 5 Comparison of the blade-internal cavity median SPL between the small and large internal domains

IV.Conclusion

A high-order computational approach was employed to investigate the damage-induced sound of flow over an airfoil for development of the wind turbine blade acoustics-based structural health monitoring approach. Based on these simulation results, three main conclusions can be drawn. First, damage located just after the transition location from laminar to turbulent flow resulted in the greatest change in flow-generated sound and would likely be easiest to detect. Second, damage located in the laminar flow region had negligible impact on the generated sound, so detection would depend on the change in transmission loss, not on the change in flow-generated sound. Finally, analysis of blade internal cavity size showed that the sound pressure levels for the small cavity case were greater than for the large cavity case, supporting the idea that damage would be easier to detect in smaller cavities. This investigation sets up future studies to continue the research into damage-induced sound. Moving forward, factors such as the Reynolds number, airfoil profile, and damage types can be varied to have a better understanding of the wind turbine acoustics problem.

Funding Sources

This material is based upon work supported by the National Science Foundation under grant number CMMI 1538100 (Acoustics-based Structural Health Monitoring of Closed-cavities and its Application to Wind Turbine Blades). Any opinions, findings, and conclusions or recommendations expressed in this material are those of the author (s) and do not necessarily reflect the views of the National Science Foundation.

Acknowledgments

This research used resources of the National Energy Research Scientific Computing Center, a DOE Office of Science User Facility supported by the Office of Science of the U.S. Department of Energy under Contract No. DE-AC02-05CH11231 using NERSC award ASCR-ERCAP0021324. The research also used the Savio computational cluster resource provided by the Berkeley Research Computing program at the University of California, Berkeley (supported by the UC Berkeley Chancellor, Vice Chancellor for Research, and Chief Information Officer).

References

1. Beale, C., Willis, D. J., Niezrecki, C., and Inalpolat, M. "Passive acoustic damage detection of structural cavities using flow-induced acoustic excitations," *Structural Health Monitoring*, 2019, p. 1475921719860389.
doi: 10.1177/1475921719860389
2. Willis, D., Niezrecki, C., Kuchma, D., Hines, E., Arwade, S., Barthelmie, R., DiPaola, M., Drane, P., Hansen, C., and Inalpolat, M. "Wind energy research: State-of-the-art and future research directions," *Renewable Energy* Vol. 125, 2018, pp. 133-154.
doi: 10.1016/j.renene.2018.02.049
3. Ciang, C. C., Lee, J.-R., and Bang, H.-J. "Structural health monitoring for a wind turbine system: a review of damage detection methods," *Measurement Science and Technology* Vol. 19, No. 12, 2008, p. 122001.
doi: 10.1088/0957-0233/19/12/122001
4. Hameed, Z., Hong, Y., Cho, Y., Ahn, S., and Song, C. "Condition monitoring and fault detection of wind turbines and related algorithms: A review," *Renewable and Sustainable energy reviews* Vol. 13, No. 1, 2009, pp. 1-39.
doi: 10.1016/j.rser.2007.05.008
5. Inalpolat, M., and Niezrecki, C. "Acoustic Sensing Based Operational Monitoring of Wind Turbine Blades," *JPhCS* Vol. 1452, No. 1, 2020, p. 012050.
doi: 10.1088/1742-6596/1452/1/012050
6. Niezrecki, C., and Inalpolat, M. "Structural health monitoring of wind turbine blades using wireless acoustic sensing," *University of Massachusetts, Boston, MA, US Patent No. PCT/US2014/062329. https://patentscope. wipo. int/search/en/detail. jsf.* 2015.
7. Beale, C., Inalpolat, M., and Niezrecki, C. "Active acoustic damage detection of structural cavities using internal acoustic excitations," *Structural Health Monitoring*, 2019.
doi: 10.1177/1475921719835761
8. Beale, C., Niezrecki, C., and Inalpolat, M. "An adaptive wavelet packet denoising algorithm for enhanced active acoustic damage detection from wind turbine blades," *Mechanical Systems and Signal Processing* Vol. 142, 2020, p. 106754.
doi: 10.1016/j.ymssp.2020.106754
9. Regan, T., Beale, C., and Inalpolat, M. "Wind Turbine Blade Damage Detection Using Supervised Machine Learning Algorithms," *Journal of Vibration and Acoustics* Vol. 139, No. 6, 2017, p. 061010.
doi: 10.1115/1.4036951
10. Solimine, J., Niezrecki, C., and Inalpolat, M. "An experimental investigation into passive acoustic damage detection for structural health monitoring of wind turbine blades," *Structural Health Monitoring*, 2020, p. 1475921719895588.
doi: 10.1177/1475921719895588
11. Solimine, J., and Inalpolat, M. "An unsupervised data-driven approach for wind turbine blade damage detection under passive acoustics-based excitation," *Wind Engineering*, 2022, p. 0309524X221080470.
doi: 10.1177/0309524X221080470
12. Traylor, C., DiPaola, M., Willis, D. J., and Inalpolat, M. "A computational investigation of airfoil aeroacoustics for structural health monitoring of wind turbine blades," *Wind Energy* Vol. 23, No. 3, 2020, pp. 795-809.
doi: 10.1002/we.2459
13. Traylor, C., and Inalpolat, M. "A generalized computational approach to predict high-frequency acoustic pressure response of cavity structures for structural health monitoring of wind turbine blades," *Wind Engineering*, 2021, p. 0309524X211060552.
doi: 10.1177/0309524X211060552

14. Traylor, C., and Inalpolat, M. "Prediction of wind turbine blade trailing edge noise under various flow conditions for a passive damage detection system," *INTER-NOISE and NOISE-CON Congress and Conference Proceedings*, Institute of Noise Control Engineering, 2021, 4079-4087.
doi: 10.3397/IN-2021-2597
15. Traylor, C., and Inalpolat, M. "Computational investigation into the effect of material properties on aeroacoustics based damage detection from wind turbine blades " *NOISE-CON 2022*, Institute of Noise Control Engineering, Lexington, KY, 2022, 317-327.
doi: 10.3397/NC-2022-736
16. Peraire, J., and Persson, P.-O. "High-order discontinuous Galerkin methods for CFD," *Adaptive high-order methods in computational fluid dynamics*. World Scientific, 2011, pp. 119-152.
doi: 10.1142/9789814313193_0005
17. Vermeire, B. C., Witherden, F. D., and Vincent, P. E. "On the utility of GPU accelerated high-order methods for unsteady flow simulations: A comparison with industry-standard tools," *Journal of Computational Physics* Vol. 334, 2017, pp. 497-521.
doi: 10.1016/j.jcp.2016.12.049
18. Wang, Z. J., Fidkowski, K., Abgrall, R., Bassi, F., Caraeni, D., Cary, A., Deconinck, H., Hartmann, R., Hillewaert, K., and Huynh, H. T. "High-order CFD methods: current status and perspective," *International Journal for Numerical Methods in Fluids* Vol. 72, No. 8, 2013, pp. 811-845.
doi: 10.1002/fld.3767
19. Visbal, M. R., and Gaitonde, D. V. "On the use of higher-order finite-difference schemes on curvilinear and deforming meshes," *Journal of Computational Physics* Vol. 181, No. 1, 2002, pp. 155-185.
doi: 10.1006/jcph.2002.7117
20. Drela, M. "XFOIL: An analysis and design system for low Reynolds number airfoils," *Low Reynolds number aerodynamics*. Springer, 1989, pp. 1-12.
doi: 10.1007/978-3-642-84010-4_1